Intracellular lipopolysaccharide binds FAM134B to regulate ER remodeling upon bacterial infection

Yi-Lin Cheng[1,2,3,4]*, João Mello-Vieira[1,2], Adriana Covarrubias-Pinto[1], Alexis Gonzalez[1], Santosh Kumar Kuncha[1,2,5], Chun Kew[1,2], Kaiyi Zhang[6], Muhammad Awais Afzal[7], Nour Diab[6], Sophia Borchert[8], Wenbo Chen[1,2], Timothy Chun Huang[3,9], Uxía Gestal Mato[1], Mathias Walter Hornef[6], Christian A. Hübner[7], Michael Hensel[8], Ivan Dikic[1,2,10,11,]*

[1]Institute of Biochemistry II, Faculty of Medicine, Goethe University, Frankfurt, Germany

[2]Buchmann Institute for Molecular Life Sciences, Goethe University, Frankfurt, Germany

[3]Institute of Basic Medical Sciences, College of Medicine, National Cheng Kung University, Tainan, Taiwan

[4]Center of Infectious Disease and Signaling Research, National Cheng Kung University, Tainan, Taiwan

[5]Altos Labs Inc, Bay Area Institute, Redwood City, CA, USA

[6]Institute of Medical Microbiology, RWTH University Hospital, Aachen, Germany

[7]Institute of Human Genetics, Jena University Hospital, Friedrich Schiller University, Jena, Germany

[8]Abt. Mikrobiologie, Universität Osnabrück, Osnabrück, Germany

[9]School of Medicine, College of Medicine, National Cheng Kung University, Tainan, Taiwan

[10]Max Planck Institute of Biophysics, Frankfurt, Germany

[11]Fraunhofer Institute for Molecular Biology and Applied Ecology (IME)

*Correspondence: dikic@biochem2.uni-frankfurt.de;

yilincheng@gs.ncku.edu.tw

ABSTRACT

Selective autophagy of the endoplasmic reticulum (ER), termed ER-phagy, plays a key role in organelle remodeling and cellular homeostasis. However, whether and how ER-phagy is regulated during Gram-negative bacteria infection to influence host responses remains unclear. Here, we show that *Salmonella enterica* serovar Typhimurium releases lipopolysaccharide (LPS) that colocalizes with FAM134B, a reticulon-like ER-resident receptor for ER-phagy. Cytosolic delivery of LPS, either during infection or via transfection, markedly increases FAM134B- and LC3B-decorated ER fragments. Mechanistically, pulldown assays demonstrate that LPS directly binds FAM134B through interactions between lipid A and positively charged residues within its amphipathic helices and C-terminal region. This interaction promotes FAM134B oligomerization and drives ER membrane fragmentation, a process further amplified by the O-antigen moiety of LPS. The resulting ER fragments accumulate around LC3-positive *Salmonella*-containing vacuoles, facilitating bacterial clearance. Importantly, both intracellular and extracellular *Salmonella* exploit outer membrane vesicles (OMVs) to deliver LPS into the host cytosol, triggering FAM134B activation and ER remodeling. Collectively, our findings reveal a previously unrecognized host response by

which LPS of Gram-negative bacteria are sensed by the host ER-phagy machinery to promote xenophagy and enhance antibacterial defense.

KEYWORDS

ER remodeling; FAM134B; lipopolysaccharide; outer membrane vesicles; *Salmonella*

Abbreviations

AH: amphipathic helix; BMDMs: bone-marrow-derived macrophages; Co-IP: Co-immunoprecipitation; BafA1: Bafilomycin A1; Cterm: C-terminal region (Cterm); CFU: colony-forming units; DAPI: 4',6-diamidino-2-phenylindole; ER: endoplasmic reticulum; EPEC: enteropathogenic *Escherichia coli*; GBP: guanylate-binding protein; IRGB10: immunity-related GTPase family member B10; KDO: Keto-3-deoxy-octonate; LPS: lipopolysaccharide; LPR: lipid-to-protein ratio; LC3B: microtubule associated protein 1 light chain 3 beta; mtLIR: LC3B-interacting region mutant; MDP: Muramyl dipeptide; OMVs: outer membrane vesicles; O-Ag: O-antigen; OmpA: outer membrane protein A**;** RHD: reticulum homology domain; R-LPS: rough-LPS; S-LPS: smooth-LPS; SFB: S-protein-FLAG-streptavidin binding peptide; TM: transmembrane domains; TEM: transmission electron microscopy; WT: wild-type; SCVs: *Salmonella*-containing vacuoles.

Introduction

Multiple intracellular Gram-negative bacteria have been identified to manipulate host membrane system, including the endoplasmic reticulum (ER), which is the most abundant

membranous system in mammalian cells [1]. However, whether there is a common component of Gram-negative bacteria participating in the regulation of ER membranes is unclear. The selective autophagy of the ER (ER-phagy) has recently been identified as the master mechanism for ER remodeling and turnover [2], enabling lysosomal degradation of different ER components, which are engulfed into autophagosomes through the interaction of microtubule associated protein 1 light chain 3 beta (LC3B) with ER-phagy receptors [2-4]. Eight mammalian ER-phagy receptors have been identified, including the FAM134 family [5-7], RTN3 [8], Sec62 [9], CCPG1 [10], ATL3 [11], TEX264 [12,13], and CALCOCO1[14], which facilitate the degradation of different ER subdomains and respond to different types of stress conditions. The FAM134 family and RTN3L, in particular, are able to induce significant ER remodeling. They contain two hairpin-like domains (transmembrane domains; TM) anchored into the lipid bilayer and connected by an amphipathic helix (AH) linker, as well as another carboxy-terminal AH, which is connected to the second TM. Together they form a reticulum homology domain (RHD), whose integrity appears critical for ER-phagy [5,8,15]. The RHD of FAM134B, the best-studied ER-phagy receptor, can sense highly positive membrane curvature, thereby triggering the formation of FAM134B clusters that provide an additional force for ER membrane budding and scission [15-18].

LPS is the main component of the outer membrane of Gram-negative bacteria. It is composed of a conserved lipid A moiety, the inner core and outer core oligosaccharides, and

O-antigen (O-Ag), the outermost part composed of a variable number of repeating sugar residues. In recent decades, most studies have focused on the extracellular role of LPS, which is specifically sensed on the plasma membrane by the Toll-like receptor 4 /myeloid differentiation factor 2 co-receptor complex, that acts in conjugation with Cluster of Differentiation 14 (CD14) to trigger signaling cascades for the expression of inflammatory genes [19]. The release of LPS by intracellular *Salmonella* to cytosolic vesicles was reported by Portillo and colleagues as early as 1997, however the targeted proteins and downstream effects are still elusive [20]. More recently, human caspase-4 (mouse homologue caspase-11) and caspase-5 have been identified as innate immune receptors that specifically recognize intracellular LPS [21]. The lipid A moiety of LPS directly binds to the amino (N)-terminal caspase-activation and recruitment domain of these caspases, triggering their oligomerization and activation [21]. Activated caspase-4/-11 further cleave gasdermin D to liberate its N-terminal domain, which has membrane-pore-forming activity at the plasma membrane and thereby induces pyroptosis [22,23]. Moreover, LPS on cytosolic *Salmonella* is also recognized by guanylate-binding protein (GBP) 1, which initiates the assembly of a GBP coat for caspase-4 recruitment and activation to trigger non-canonical inflammasome signaling [24].

Extracellular Gram-negative bacteria also expose LPS to the cytosol, by having their LPS-enriched outer membrane vesicles (OMVs) internalized into the cell [25]. The bacterial envelop is composed of the cytoplasmic membrane and the outer membrane, which enclose

the periplasmic space containing a peptidoglycan layer and periplasmic proteins that stabilize the membrane through various crosslinks [26-28]. Upon infection, environmental stress factors released by the host disturb the stability of those crosslinks and increase outer membrane budding into OMVs with a diameter of 20 nm to 250 nm. OMVs are internalized into the host cell via endocytosis, and LPS is released from early endosomes into the cytosol, where it activates caspase-11 [25] and possibly exerts other effects.

Here we describe a novel function for intracellular LPS mediated by binding to FAM134B ER-phagy receptor. Both *Salmonella* infection and intracellular LPS induced FAM134B-mediated ER fragmentation. *Salmonella* LPS colocalized with FAM134B as determined by immunofluorescence experiments, and biochemical analysis showed that lipid A of LPS directly bound to FAM134B via electrostatic forces. Although lipid A was sufficient for FAM134B binding, oligomerization of FAM134B and the following membrane fragmentation required the presence of O-Ag of LPS. FAM134B-associated ER membrane then surrounded xenophagosomes promoting bacterial clearance. We also found that OMVs are responsible for the delivery of LPS from both intracellular and extracellular bacteria into the cytosol. Taken together, this study identified FAM134B as an intracellular sensor of LPS, enabling the ER membrane remodeling and xenophagy.

Results

LPS colocalizes with FAM134B and triggers FAM134B-mediated ER fragmentation

To investigate whether intracellular Gram-negative bacteria activate ER-phagy, we first examined the role of the ER-phagy receptor FAM134B during *Salmonella enterica* serovar Typhimurium SL1344 infection. In HeLa TREx FLAG-HA-FAM134B-inducible cells, *Salmonella* infection strongly induced colocalization of FAM134B puncta with LC3B puncta, indicating induction of FAM134B-mediated ER fragmentation upon infection (Figure 1A). Comparing to FAM134B, RTN3 did not show significant colocalization with LC3B after *Salmonella* infection (Figure S1A). To our surprise, we found LPS puncta colocalizing with FAM134B which were not associated with bacteria, indicated by nucleic acid staining with 4',6-diamidino-2-phenylindole (DAPI), either in wild-type (WT) FAM134B or LC3B-interacting region mutant (mtLIR) FAM134B (Figure 1A and Figure S1B). Moreover, endogenous FAM134B, also colocalized with *Salmonella* LPS after infection (Figure S1C). High throughput analysis by confocal imaging cytometer CQ1 showed that around 20% of LPS puncta colocalized with FAM134B after *Salmonella* infection (Figure 1B). Despite most of FAM134B puncta colocalize with LPS or LC3B, respectively (arrows), some of FAM134B puncta colocalize with LPS and LC3B simultaneously (arrowheads) as the histogram showed (Figure 1A). The number of FAM134B/LC3B-positive puncta after *Salmonella* infection was significantly increased in WT FAM134B-expressing HeLa cells, but not in mtLIR FAM134B-

expressing HeLa cells, indicating *Salmonella* infection caused induction of FAM134B-mediated ER-phagy and ER fragmentation (Figure 1C and Figure S1D). Co-immunoprecipitation (Co-IP) assays revealed that *Salmonella* infection enhanced interaction of FAM134B with LC3B-II in the presence or absence of Bafilomycin A1 (BafA1), which inhibits maturation of autophagosomes for lysosomal degradation (Figure 1D). Our previous study defined ER fragments as puncta containing FAM134B, LC3B-II and ER proteins that do not directly bind LC3B [18]. To clarify whether LPS can trigger FAM134B-mediated ER fragmentation, we transfected *Salmonella* LPS in HeLa cells followed by immunostaining and confocal microscopy analysis. The results showed that LPS colocalizes with FAM134B puncta and LC3B puncta simultaneously (arrowheads) showing in the images and the histogram (Figure 1E). The number of FAM134B/LC3B-positive puncta also increased in presence of LPS (Figure 1F). Moreover, transfection of *Salmonella* LPS triggered FAM134B fragments delivered to lysosomes, indicated by LAMP1 (Figure S1E). Thus, *Salmonella* LPS initiated FAM134B-mediated ER fragmentation.

LPS binds to FAM134B via electrostatic force

Since LPS colocalized with FAM134B in the confocal images, we hypothesized that LPS binds directly to FAM134B. Therefore, we carried out a series of streptavidin pull down assays to clarify the mode of interaction (Figure 2A). We used biotin-conjugated *E. coli* O111:B4 LPS immobilized on streptavidin sepharose to study its interaction with either HA-

FAM134B or HA-RTN3L (Figure 2B). We detected that biotin-LPS strongly pulled down HA-FAM134B in a dose-dependent manner, while contained much less affinity to HA-RTN3L (Figure 2B). The endogenous FAM134B in the lysates of HeLa cell also was pulled downed by biotin-LPS strongly compared to the other ER-phagy receptors, RTN3L and TEX264 (Figure 2C). The binding of LPS to FAM134B was LIR motif-independent (Figure S2A). In addition to *in vitro* pulldown assays, pulling down the biotin-LPS which delivered into cells expressing FLAG-HA-FAM134B or FLAG-HA-RTN3L also showed strong interaction to FAM134B (Figure S2B). Upon *Salmonella* infection in cells expressing FLAG-HA-FAM134B, immunoprecipitation of HA-FAM134B was also able to detect the interaction of LPS, but no significant interaction between RTN3L and LPS was detected upon *Salmonella* infection (Figure 2D). To further clarify which segment of LPS is required for binding to FAM134B, we performed a competition assay. WT LPS (also called smooth (S)-LPS), rough LPS, including Ra-LPS (LPS without O-Ag) and Re-LPS (LPS containing lipid A and three 2-Keto-3-deoxy-octonate (KDO)), and lipid A (Figure 2E), were preincubated with lysates containing FLAG-HA-FAM134B, followed by incubation with biotin-LPS-immobilized streptavidin sepharose. We analyzed whether the preincubation with different LPS variants can block the binding of biotin-LPS to FAM134B (Figure 2F). The results revealed that all kinds of LPS significantly reduced the binding ability of biotin-LPS to FAM134B, except Muramyl dipeptide (MDP), which is another component of the bacteria cell wall,

demonstrating that lipid A is sufficient for FAM134B binding (Figure 2F). Furthermore, polymyxin B, a cationic peptide antibiotic, which interacts with lipid A via ionic and hydrophobic forces, inhibited the binding of biotin-LPS to FAM134B in a dose-dependent manner (Figure 2G).

Next, we characterized how FAM134B binds to LPS. Since lipid A contains multiple negatively charged groups [29], we hypothesized that the interaction might occur through electrostatic forces. We analyzed each domain of FAM134B and found that two cytoplasmic amphipathic helices, the linker and C-terminal region of the amphipathic helices (AHL and AHC), and the C-terminal region (Cterm), are highly solvent-accessible and enriched with positively charged residues, including arginine (R) and lysine (K) (Figure 3A). According to this analysis, we mutated R or K residues to glutamic acid (E) in these three FAM134B regions (Figure 3B). We then evaluated the interactions of these mutants with biotin-LPS. Each mutant FAM134B construct showed significantly reduced binding to biotin-LPS, and binding was completely abolished when mutations in all three regions were combined (Figure 3C). Transfection of FAM134B TRIPLEmt (mutations in all three regions) robustly blocked colocalization of FAM134B with LPS and LC3B (Figure 3D, E). These results were also confirmed by Co-IP experiments in which FAM134B TRIPLEmt-HA co-precipitated significantly less LPS and LC3B-II compared to FAM134B WT-HA (Figure 3F). Moreover, *in vitro* streptavidin pulldown assays showed that biotin-LPS pulled down FAM134C and

FAM134B with similar efficiency whereas FAM134A interacted significantly weaker (Figure S2C). This result could be explained by the fact that FAM134B and FAM134C have a high sequence similarity, from which the sequence of FAM134A clearly deviates (Figure S2D, E, F).

FAM134B oligomerization is triggered by O-Ag of LPS

Oligomerization of FAM134B is reported to drive ER membrane scission followed by ER-phagy induction [17]. Especially, caspases also undergo oligomerization after binding with LPS [21]. We therefore hypothesized that LPS binds to FAM134B to induce its oligomerization. S-protein-FLAG-streptavidin binding peptide (SFB)-FAM134B was expressed and purified from HEK293T cells followed by incubation with S-LPS or lipid A. In order to analyze oligomeric species of FAM134B, we performed blue native PAGE, which enforces migration of native protein complexes or oligomers based solely on their molecular weight [30], followed by immunoblotting with FLAG. S-LPS significantly increased the presence of FAM134B oligomers of approximately 720 kDa (Figure 4A). To our surprise, lipid A did not show a similar effect, although it played a major role in binding to FAM134B, suggesting that O-Ag is indispensable for the oligomerization of FAM134B. To test this idea, we infected HeLa cells expressing SFB-FAM134B with an isogenic set of *Salmonella* mutant strains with defined defects in the O-antigen biosynthesis, including the *rfbP* (O-antigen transferase) and *rfaL* (O-antigen ligase) mutant strains lacking O-Ag, the *rfaG*

(glucosyltransferase I) mutant strain lacking O-Ag and outer core, as well as the *rfaH* (transcriptional activator) mutant strain with reduced polymeric O-Ag (Figure 4B, C) [31]. After infection, SFB-FAM134B was purified, and blue native PAGE analysis was performed. The results showed that FAM134B oligomers in the range of ~720 kDa to ~1048 kDa were significantly reduced after infection with any of the O-Ag-defective strains compared to WT and complemented strains (Figure 4B).

FAM134B clustering would further induce membrane curvature and remodeling [15]. To further prove that O-Ag regulates membrane remodeling driven by FAM134B, we conducted a liposome-remodeling assay in which incubation with purified FAM134B drives membrane fragmentation [15]. We first determined the suitable lipid-to-protein ratio (LPR) for the examination of the effect of LPS on FAM134B-triggered membrane fragmentation (Figure S3A, B). LPR 40:1 triggered strong liposome remodeling, indicated by a significant reduction of the liposome diameter compared to the control group of liposomes only (Empty). LPR 100:1 had a moderate effect, resulting in a slightly reduced liposome size (Figure S3A, B). Thus, we used LPR 100:1 to study the action of LPS (Figure 4D, E, F, G). S-LPS significantly enhanced the membrane remodeling effect of FAM134B compared to liposomes incubated with FAM134B alone in a dose-dependent manner (Figure 4D, E). Notably, LPS alone did not change the size of liposomes compared to the control sample, demonstrating that LPS cannot fragment membrane by itself, but enhances the action of FAM134B on membranes (Figure

4D, E). Compared to S-LPS, Ra-LPS and Re-LPS, which lack the O-Ag, had less pronounced effects on the size of liposomes, i.e. on the ability of FAM134B to induce membrane fragmentation (Figure 4F, G). To further verify the role of O-Ag in ER fragmentation in cells, we performed co-localization analysis of HA-FAM134B and LC3B after infection of WT, the isogenic mutant strains without O-Ag, and the two complemented strains of Δ*rfaL* and Δ*rfaG* (Figure 4H, S3C). The number of FAM134B/LC3B-positive puncta was significantly reduced upon infection with O-Ag mutant strains, Δ*rfbP,* Δ*rfaL,* Δ*rfaG,* and Δ*rfaH* strains, in comparison to the WT strain. On contrary, complemented strains of Δ*rfaL* and Δ*rfaG* induced a similar number of FAM134B/LC3B-positive puncta as the WT strain (Figure 4H, S3C). The bacteria count per cell did not show significant differences among the groups at this early time point, implying the reduction in FAM134B/LC3B-puncta was not due to fewer bacteria (Figure 4I, S3C). Compared to S-LPS, transfection of Ra-LPS, Re-LPS, and lipid A, which are the LPS without O-Ag, did not increase the number of HA-FAM134B/LC3B-positive puncta (Figure S3D, E). The other two cell wall components of bacteria, Pam3CSK4 and MDP, did not affect puncta formation (Figure S3D, E). These results demonstrated that O-Ag of LPS triggered oligomerization of FAM134B and FAM134B-mediated membrane remodeling.

FAM134B is recruited to xenophagosomes and promotes bacterial clearance

To further investigate the fate and function of FAM134B after infection, we measured the FAM134B-mediated ER-phagy flux by mCherry-EGFP-FAM134B WT or LIR mutant-inducible HeLa cells after *Salmonella* infection for 2 hr and 4 hr (Figure S4A, S4B). Owing to the instability of EGFP in acidified environment, only the red fluorescence of mCherry would be detected when FAM134B is delivered to lysosomes [5,13,17]. *Salmonella* infection strongly induced formation of red FAM134B puncta 4 hr post-infection in mCherry-eGFP-FAM134B WT HeLa cells, but not in cells expressing the LIR mutant (Figure S4A, S4B). Moreover, FAM134B which is positive for both GFP and mCherry forming vacuoles surround bacteria (Figure S4A-1). In *Salmonella*-infected intestinal tissue sections of 5 days-old suckling mice, FAM134B was also recruited to *Salmonella* (Figure S4C). The FAM134B-positive *Salmonella*-containing compartments were positive for ER markers, calnexin and REEP5 as well (Figure S4D).

According to previous studies, invasive *Salmonella* can survive in the endolysosomal membrane-derived *Salmonella*-containing vacuoles (SCVs), but some populations of bacteria escape into cytosol, which can be cleared after sequestration in xenophagosomes or become hyperproliferating bacteria [32-36]. We decided to study whether the FAM134B-positive structures contribute to one of these two compartments. We observed that bacteria decorated with FAM134B-HA, can colocalize with LC3B but not with the endolysosomal marker LAMP1 (Figure 5A). The imaging analysis showed the percentage of LC3B-positive and

FAM134B-positive *Salmonella* are similar, and both significantly accumulated after Baf A1 treatment, indicating these vacuoles underwent lysosomal degradation (Figure 5B). LAMP-1-positive SCVs accounts around 40% of total *Salmonella*, which did not change obviously after Baf A1 treatment at 2 hr post-infection, and even reduced at 4hr post-infection (Figure 5B). The imaging analysis further showed almost 60% LC3B-positive *Salmonella*-containing xenophagosomes were FAM134B-positive after *Salmonella* infection for 2 hr, and around 40 % at 4 hr post-infection; conversely very few SCVs, labeled by LAMP-1, were FAM134B-positive (Figure 5C). To further confirm whether FAM134B contribute to xenophagosomes formation, the numbers of xenophagosomes were counted in FAM134B WT and FAM134B KO HeLa cells. The results revealed that the numbers of xenophagosomes indicated by LC3B staining reduced in FAM134B KO cells (Figure 5D, E). Moreover, ER marker, REEP5 also showed stronger colocalization with LC3B in WT cells compared to FAM134B KO cells (Figure 5D). In FAM134B KO mouse bone-marrow-derived macrophages (BMDMs), REEP5-surrounded *Salmonella* also significantly reduced compared to WT BMDMs (Figure S4E-G). Since xenophagy machinery usually recognizes cytosolic *Salmonella* for clearance, we further detected bacterial growth. The plating assay showed that the colony-forming units (CFU) significantly increased in FAM134B KO HeLa cells compared to WT cells after *Salmonella* infection (Figure 5F). The imaging analysis revealed the multiplication of cytosolic *Salmonella*, which only expressed green florescence in cytosol, increased in

FAM134B KO HeLa cells compared to WT cells (Figure 5G,H). These results suggest that host cells use FAM134B-associated ER membrane to promote xenophagosomes formation for bacterial clearance.

OMVs are required for LPS delivery to induce FAM134B-mediated ER remodeling

Transmission electron microscopy (TEM) studies revealed that LPS secreted by *Salmonella* is presented on vesicular structures that resemble OMVs generated by bacteria [20]. OMVs, which are enriched in LPS on the surface, are also responsible for delivery of LPS from extracellular bacteria to the host cell cytosol via endocytosis [25]. Hence, we investigated whether OMV production is required for FAM134B-mediated ER fragmentation. OMV production is governed by various mechanisms that detach the outer membrane from the underlying peptidoglycan and then allow outward budding to form vesicles [27,28]. For example, the outer membrane protein A (OmpA) is the major outer membrane porin in *E. coli* and *S. enterica* and is linked to peptidoglycan. Lack of OmpA results in decreased stability of the outer membrane and increased release of OMVs, which has been previously reported for *S. enterica* serovars Typhimurium [37] and Typhi [38], and was confirmed for the mutant strains used in our study by ultrastructural analyses (Figure S5A,B,C). Another example is TolAB, which encodes components of the multi-subunit Tol-Pal complex that controls the constriction of the cell envelope during cell division. Mutant strains lacking TolAB show increased OMV production due to defects in partitioning the outer membrane during cell elongation and

septation [39]. DegS is also involved in OMV production. It is part of a sensor system responding to periplasmic stress, which is, for example, induced by accumulation of misfolded secretory proteins. If the stress response system is absent, the accumulation of misfolded proteins in the periplasm induces increased OMV production to remove toxic aggregates [38]. On the contrary, PagL is a deacylase that removes one lipid from hexa- or hepta-acylated lipid A of LPS [40]. This modification alters topology of LPS in the outer membrane, resulting in increased membrane curvature and OMV release [41]. We therefore established *Salmonella* strains mutated in the genes *pagL*, *ompA*, *tolAB*, and *degS*, and obtained the images of OMVs production by scanning electron microscopy (SEM) and TEM followed by measurement of OMVs amount and size distribution (Figure S5A, B, C). Compared to the WT strain, the Δ*ompA*, Δ*tolAB*, and Δ*degS* strains showed increased production of OMVs. Conversely, no vesicles could be detected with the Δ*pagL* strain (Figure S5C), which is in line with previous findings showing that deletion of *pagL* results in decreased generation of OMVs by intracellular *Salmonella* [41].

Mutation of *ompA*, *tolAB*, and *degS*, associated with increased OMVs production, augmented the number of FAM134B/LC3B-positive puncta to varying degrees (Figure 6A and S5D). Especially, mutation of *tolAB* strongly increased puncta formation compared to the WT group. Conversely, the number of FAM134B/LC3B-positive puncta decreased when *pagL* was mutated (Figure 6A and S5D). The LPS levels in the cell lysates and the amount of LPS

interacting with FAM134B positively correlated with the number of FAM134B/LC3B-positive puncta (Figure 6A, C). The bacterial counts for the different isogenic mutant strains did not show significant change at 2 hr post-infection (Figure 6B). To further explore whether OMVs can directly activate FAM134B-mediated ER fragmentation, we purified OMVs from *Salmonella* and treated HeLa TREx FLAG-HA-FAM134B cells with these OMVs. After treatment with *Salmonella* OMVs, we observed colocalization of LPS and HA-FAM134B. The number of FAM134B/LC3B-positive puncta also increased (Figure 6D, E). To differentiate whether FAM134B mainly bound to shed LPS or the LPS on OMVs, we stained OMVs by Vybrant DiO dye after purification and then treated the cells. Confocal microscopy showed that FAM134B mainly colocalized with the LPS free from the Vybrant DiO-positive OMVs (Figure S6A). Nevertheless, whether FAM134B interact with the OMVs or the outer membrane of *Salmonella* still need to be further investigated. Especially, we found that the bacterial outer membrane proteins, such as SlyB and OmpA, are identified in the interactome of FAM134B during *Salmonella* infection (Figure S7A, B, C). The gene ontology analysis of the bacterial proteins identified by FAM134B-interactome also showed highly correlation with bacterial cell outer membrane components (Figure S7D). Furthermore, the O-Ag mutant strains-derived OMVs lost the ability to trigger FAM134B-mediated ER fragmentation (Figure 6F). We further tested whether extracellular bacteria, more specifically Enteropathogenic *Escherichia coli* (EPEC), can induce a similar phenomenon. In addition to

direct exposure, transwells with 0.45 μm polycarbonate membranes were used to prevent bacteria passage but allow OMVs transition. The results reveal that EPEC induced similar amount of FAM134B/LC3B-positive puncta in direct infection and transwell system (Figure 6G, H). The *E. coli* strain without O-Ag, BL21, was used as the negative control, showing no significant formation of FAM134B puncta (Figure 6G, H). The number of LC3B-decorated FAM134B puncta also increased in the cells with EPEC-derived OMVs, which were pre-stained by Vybrant DiO after purification. However, BL21-derived OMVs did not cause same effect (Figure 6I and S6B). These results suggest that intracellular and also extracellular bacteria utilize OMVs for the delivery of LPS to activate FAM134B-mediated ER fragmentation.

Discussion

In this study, we demonstrate that FAM134B, an ER-phagy receptor, directly interacts with LPS to induce ER membrane fragmentation and promote the formation of ER membrane-associated xenophagosomes. This interaction is predominantly mediated by lipid A moiety of LPS and positively charged amino acid residues within FAM134B. Additionally, O-Ag component of LPS appears to be critical for oligomerization of FAM134B and the subsequent membrane fragmentation, although the precise molecular dynamics of this process remain to be elucidated.

Previously we reported that the RHD of FAM134B forms wedge-shaped membrane inclusions that induce membrane curvature followed by membrane fragmentation [15]. In our recent study [18] We further showed that ubiquitination of the RHD fine-tunes this membrane remodeling activity, enhancing large-scale membrane deformation, increasing receptor clustering, and promoting ER-phagy flux. Here, we find that mutations of multiple lysine residues of FAM134B, previously identified as ubiquitination sites, significantly impair LPS binding (Figure 2). This suggest that LPS may functionally utilize ubiquitination in facilitating FAM134B oligomerization and membrane fragmentation.

The ability of LPS to directly engage FAM134B and induce ER-phagy supports a model wherein *Salmonella* infection activates ER-phagy to supply membranes for xenophagosome formation. Our knockdown experiments indicate that depletion of FAM134B reduces xenophagosome formation, potentially allowing bacterial multiplication. Recently, Gatica *et al*. also showed that *Salmonella* inhibits starvation-induced ER-phagy by affecting FAM134B oligomerization, and that FAM134B controls *Salmonella* infection through unknown mechanisms [42]. Their study, performed in starved HEK293T cells with elevated baseline ER-phagy, identified the *Salmonella* effector SopF as a negative regulator of FAM134B oligomerization via ADP-ribosylation. In contrast, we did not detect SopF among the FAM134B interactors in our system (Figure S7A–C), suggesting that *Salmonella* may differentially deploy effectors depending on the host cell type or its nutritional and autophagic

status. Indeed, CFU assays revealed a ten-fold higher bacterial load in HEK293T cells compared to HeLa cells. The discrepancy may reflect the opposing modes of FAM134B regulation, suppression in HEK293T versus activation in HeLa cells, underlying distinct infection outcomes [42]. Future studies should explore whether SopF interferes with LPS-induced ER-phagy directly.

Beyond its role in vacuole formation, this ER remodeling pathway likely serves additional functions. The ER is a central hub for various physiological processes, including vesicular trafficking, the unfolded protein response (UPR), ER-lysosome associated degradation, and ER-organelle contact-site formation [2]. Dynamics reshaping of the ER enables cells to adopt to stress conditions, for instance, Gram-positive bacterial infections trigger stress via activation of the innate sensor stimulator of interferon genes (STING), while simultaneously induces autophagy [43]. Upon these conditions, ER proteins co-fractionate with LC3B, suggesting activation of ER-phagy as a homeostastic response [43]. Whether FAM134B-mediated ER remodeling contributes to analogous responses during Gram-negative bacterial infection remains an intriguing question for future investigation.

Our immunofluorescence experiments showed that the FAM134B puncta predominantely colocalized with LPS that was not associated with OMVs (Figure S6A). While the precise nature of this free LPS remains unclear, insights can be drawn from studies on the guanylate-binding protein GBP1. GBP1 binds directly to lipid A in LPS micelles or on

bacterial surfaces and undergoes O-Ag-dependent polymerization [44,45]. Analogously, we observed that FAM134B binds lipid A moieties and requires O-Ag for oligomerization. Moreover, FAM134B localized not only to secreted LPS, likely present in micellar form, but also to the bacterial surface, thus mirroring GBP1 behavior. We also detected LPS puncta at early infection stages, before substantial bacterial accumulation, raising questions about the source and mechanism of early LPS release. Several studies suggest that GBPs, along with IRGB10, are instrumental in LPS release into the host cytosol. GBPs are recruited to intracellular pathogens and disrupt pathogen-containing vacuoles, releasing bacteria and their ligands into the cytosol [46]. Subsequently, GBPs recruit IRGB10 to the bacterial surface, disrupting the bacterial cell membrane and releasing bacterial ligands, including LPS [47]. Although we observed a correlation between OMV production by *Salmonella* mutants and intracellular LPS levels, the precise mechanisms governing OMV-mediated LPS release inside host cells remain to be clarified.

In summary, we identify FAM134B as a novel LPS-binding protein that undergoes oligomerization upon LPS engagement, thereby triggering ER fragmentation and promoting the formation of ER-derived xenophagosomes. Our findings uncover a previously unrecognized host cell response, in which the ER undergoes remodeling by direct interaction of LPS with ER-phagy receptor during Gram-negative bacterial infection. This work opens new avenues for understanding how host membrane dynamics regulated in response to

bacterial infection and highlights FAM134B as a potential target for modulating ER-phagy during infection.

Materials and methods

Mammalian cell culture

HeLa and HEK293T cells were obtained from American Type Culture Collection (ATCC). WT and Fam 134b KO MEFs and BMDMs were isolated from respective mice genotypes. Animal experiments are approved by the Thüringer Landesamt für Lebensmittelsicherheit und Verbraucherschutz (TLV) (license number UKJ 22-019). MEFs were isolated and cultured from E13.5 stage embryos and SV40 large T antigen plasmid was used to immortalize MEFs. To culture BMDMs, femur and tibia bones were isolated from 12–16-week-old WT and Fam134b KO mice after euthanasia. The bones were cleaned, sterilized, and the bone marrow was flushed out with sterile PBS. It was centrifuged and re-suspended with BMDM culture media (DMEM supplemented with 10% fetal bovine serum, 1% penicillin/streptomycin and 20 ng/mL of murine macrophage colony-stimulating factor) and plated in petri dishes. Fresh media was added on day 2. By day 5, differentiated macrophages were attached and the debris were removed, the cells were washed with 1x PBS, collected, counted, and plated for the experiments. Flp-In HeLa TREx cell lines (Invitrogen) were used to generate inducible cell lines by cloning the cDNAs of FAM134B, FAM134B mtLIR

(DDFELLD LIR substituted by seven alanine residues), and RTN3L into MSCV iTAP N-FLAG-HA retroviral vector. Then, 2 μg/ml puromycin and 15 μg/ml blasticidin were treated for selection and maintenance of stable cells. Cells were cultured in Dulbecco's Modified Eagle's Medium (DMEM) supplemented with 10% fetal bovine serum, 1% penicillin/streptomycin at 37°C with 5% CO2. BMDMs were additionally supplemented with 20 ng/mL of murine macrophage colony-stimulating factor (Miltenyi BioTech).

Microbe strains

S. Typhimurium strains used in this study. The following isogenic mutant and complemented NCTC12023 strains were established by Prof. Dr. Michael Hensel [31].

1. SL1344 (WT)
2. NCTC12023 (WT)
3. NCTC12023 strains with deletion on *ompA, tolAB, degS* or *pagL*.

Mutant strains of *S. enterica* serovar Typhimurium strain NCTC12023 were generated by Red-mediated homologous recombination basically as described before [48], using pWRG730 as helper plasmid for controlled expression of Red functions [49]. The 60-mer oligonucleotide sets as listed in Table X were used to amplify the *aph* targeting cassette

using pKD13 (for *tolA*, *degS*, or *ompA*) or pKD4 (for *pagL*) as template DNA. Proper insertion of *aph* cassettes into target genes was confirmed by colony PCR using gene-specific check primers flanking deletions, and universal K1 Red Del. Confirmed mutated alleles were moved into fresh strain background using P22 transduction. The effects of mutations on outer membrane integrity were analysed by SEM and nsTEM of strains grown overnight on LB agar (Extended Data Fig. 7)

4. NCTC12023 strains with deletion on *rfbP, rfaL, rfaG,* or *rfaH.*

Mutant of *rfbP* (O-Ag transferase; NP_461027; Δ*rfbP*) and *rfaL* (O-Ag ligase; NP_462613; Δ*rfaL*) are defective in the addition of the O-Ag to the outer core. Mutant of *rfaG* (glucosyltransferase I; NP_462622; Δ*rfaG*) caused outer core cannot be added to inner core. Mutant of *rfaH* (transcriptional activator; NP_ 462862; Δ*rfaH*), which is the gene regulates the stability of the long mRNA for LPS biosynthesis genes, also reduced polymeric O-Ag.

5. NCTC12023 strains with complementation of deletion of *rfaL* and *rfaG*

6. pHut-gfp *S.* Typhimurium SL1344 bacteria (express GFP when cytosolic)

E. coli strains used in this study.

1. NEB Turbo

2. EPEC O127:H6 (A kind gift from Prof. Dr. Volkhard A. J. Kempf)

3. BL21

Chemically competent NEB Turbo cells were used for plasmid amplification.

Bacterial infection

S. Typhimurium and *E. coli* were cultured overnight and then diluted at ratio of 1 to 33 in fresh LB broth. The diluted cultures were then grown at 37°C for 3 h. For infection, the resuspended bacteria were adjusted to OD600 of 1 and added to HeLa cells or MEFs at a MOI of 100, and BMDMs at a MOI of 10 without antibiotics. After 30 min of infection, media were replaced by medium with 100 μg/ml gentamicin to remove extracellular bacteria. Samples were collected at the indicated time points after infection. For colony forming assay, which was performed as previously described [50], after 10 min of *S.* Typhimurium infection, the cells were washed by PBS twice to removed extracellular bacteria and incubated in antibiotics-free DMEM for 20 min. Then, the media were changed to DMEM containing 50 μg/ml gentamicin for 40 min and replaced by DMEM containing 5 μg/ml gentamicin. The cells were lysed with lysis buffer (1% Triton X-100 and 0.1% SDS in PBS) at indicated time points and serial diluted by PBS and plated onto LB plates. After 24 h incubation at 37°C, the colonies were calculated.

Immunofluorescence staining and confocal imaging

Cells which seeded in the 6-well plates with cover slips fixed by 4% paraformaldehyde in PBS for 15 min at room temperature. The buffer with 0.1% saponin, 1% bovine serum albumin (BSA), 0.05% NaN3 in PBS was used for permeabilization and blocking for 1 h at room temperature. Samples were then probed by indicated primary antibodies as well as Alexa 488, Alexa 546, and Alexa 633 fluorescently labelled secondary antibodies (Invitrogen). After DAPI staining for nucleus and bacteria DNA, the samples were fixed by mounting medium. Confocal imaging was done using a Zeiss LSM 780 confocal microscope and analyzed by Zeiss Zen (black edition) software. For high-throughput confocal imaging, cells were seeded in the 96-well black plates with glass bottom followed by immunofluorescence staining and imaging by CellVoyager CQ1 (Yokogawa) system and quantified using CellPathfinder software (version 3.06.01.08).

Immunoprecipitation and western blotting

For immunoprecipitation, cells were lysed by the lysis buffer containing 50 mM Tris-HCl (pH 7.5),150 mM NaCl, 5 mM EDTA, and 1% NP-40 with protease inhibitor cocktail (Sigma Aldrich). Lysates were incubated with 15 μl anti-HA agarose beads (SantaCruz Biotechnology) overnight at 4°C with end-to-end rotation. Beads were washed three times

with wash buffer containing 50 mM Tris-HCl (pH 7.5), 400 mM NaCl, 5 mM EDTA). Proteins were eluted with 2X loading dye by boiling for 10 min followed by western blotting. For western blotting, cells were lysed by the lysis buffer containing 50 mM Tris-HCl (pH 7.5), 150 mM NaCl, 5 mM EDTA, and 1% Triton X-100 with protease inhibitor cocktail (Sigma Aldrich). After protein quantification, samples were boiled with loading dyes for 10 min. Samples were separated by running SDS-PAGE with Tris-Glycine gels followed by transferred to PVDF membranes, which were then blocked with 5% milk in TBST. After blocking, the membranes were sequentially hybridized with primary and HRP (horseradish peroxidase) conjugated secondary antibodies. the chemiluminescence method was performed to detect proteins expression.

Transfection of siRNA

Cells were seeded in the 6-well plates on a day before experiments. FAM134B siRNA and Scramble siRNA (Eurofins) were transfection by lipofectamine RNAiMAX (Invitrogen) as manufacturer's instruction. After 48 hr culture, cells were reseeded for the following experiments.

Streptavidin pulldown assay

To immobilize LPS onto streptavidin agarose beads, the indicated amount of biotin-conjugated *E. coli* O111:B4 LPS (InvivoGen) were added to 10 μl of streptavidin agarose beads and incubated at 4°C with rotation for 1 hr. The beads were then washed 3 times with the lysis buffer containing 50 mM Tris-HCl (pH 7.5), 150 mM NaCl, 5 mM EDTA, and 1% NP-40 to remove unconjugated ligands. Inducible TREx HeLa cells of FLAG-HA-FAM134B and FLAG-HA-RTN3 induced by treatment of 1 μg/ml doxycycline for 24 hr or HEK cells transfected with indicated plasmids were lysed and collected in the lysis buffer supplemented with a protease inhibitor mixture. Cell lysates were precleared by incubating with streptavidin Sepharose at 4°C with rotation for 1 hr. Supernatants were transferred to a new microtube and incubated with biotin-LPS-immobilized streptavidin agarose beads overnight at 4°C with rotation. The beads were then washed three times with wash buffer containing 50 mM Tris-HCl (pH 7.5), 400 mM NaCl, 5 mM EDTA and eluted in 2X loading dye by boiling for 10 min followed by western blotting to detect the binding proteins. For competition assay, 50 μg of unlabeled S-LPS, Ra-LPS, Re-LPS, lipid A, and MDP were first incubated with pre-cleared lysates at 4°C for 1 hr with rotation before adding biotinylated LPS-immobilized streptavidin beads. For examination of polymyxin B effect, the indicated concentrations of polymyxin B were first added to biotinylated LPS-immobilized streptavidin beads and incubate with rotation for 0.5 hr. After twice washes by lysis buffer, the pre-cleared lysates were added.

FAM134B protein purification

For purification of FAM134B protein from HEK293T cells, the plasmid of S protein-FLAG-Streptavidin binding peptide (SFB)-FAM134B was transfected to HEK293T cells. Cells were lysed with the lysis buffer containing 50 mM Tris-HCl, pH 7.4,150 mM NaCl, 0.5 mM EDTA, and 1% TritonX-100. After centrifuge at 17,000 g, 15 min, the lysates were collected and incubated with streptavidin Sepharose (Cytiva) at constant agitation at 4 °C, overnight. After washing three time with the buffers (50 mM Tris, pH=7.4,150 mM NaCl, 0.5 mM EDTA) containing 0.5 % NP-40, 0.3 % NP-40 and 0.1 % NP-40, respectively, the buffers were removed and the SFB-FAM134B protein on the Sepharose was further eluted by incubated with 2 mM D-biotin dissolved in the buffer containing 50 mM Tris-HCl, pH 7.4,150 mM NaCl, 0.5 mM EDTA, and 0.1% NP-40 for 1 hr at 4°C with constant agitation at 800 rpm. The eluted SFB-FAM134B was collected for blue native page analysis.

Recombinant GST-FAM134B was purified from *E. coli* for Liposome-remodeling assay as previous described [18]. Briefly, Fam134B-GST plasmids were transformed into BL21DE3 strain of *E. coli*, and a single colony was used to grow the primary culture in the presence of appropriate antibiotic (ampicillin). The overnight grown primary cultures were used to inoculate secondary cultures and allowed to grow up to a OD of 0.6 by shaking at 200 rpm and 37 °C, followed by induction of the cultures using 0.5 mM of IPTG for 3 hours. The cells

were harvested, suspended in ice cold PBS and lysed using sonication, centrifuged (10,000 xg) to separate the supernatant and pellet. The resultant supernatant was further fractioned by ultracentrifugation at 80,000g for 100 minutes at 4 °C. The pellet fractions were dissolved in PBS buffer containing dodecyl β-D-maltoside (DDM; 0.05%), followed by affinity purification using glutathione-Sepharose TM4 Fast Flow columns (GE Healthcare). The protein was eluted from the column using PBS containing 10 mM reduced glutathione and 0.05% DDM. The fractions containing Fam134B-GST protein were concentrated and buffered exchanged with storage buffer (50 mM HEPES pH 7.5, 150 mM NaCl) containing 0.0075%DDM.

Blue native page

Blue native page analysis was performed as previous described with slight modifications [17,30]. SFB-FAM134B protein was incubated with indicated amount of S-LPS or lipid A at 37°C for 2 hr. Then, the mixture was incubated with 2 μl 50% glycerol and 3 μl 0.1% Coomassie blue G-250 for 15 min at room temperature followed by loading to 4%–12% gradient native PAGE gel (Bio-Rad), running in blue cathode/anode buffer (Invitrogen) for 2 hr at 150 V in an ice bath. The gels were further transfer to PVDF membranes by electroblotting followed by detection with anti-FLAG antibody.

Liposome preparation

Liposomes were prepared as previous described [15]. In brief, two kinds of lipids,1,2-dioleoyl-sn-glycero-3-phosphocholine (DOPC, Avanti Polar Lipids Inc.) and 1,2-dioleoyl-sn-glycero-3-phosphoethanolamine (DOPE, Avanti Polar Lipids Inc.), were dissolved in a mixture of chloroform and methanol (4:1) in a glass flask to obtain the molar ratio of 0.8:0.2 (DOPC:DOPE). The organic solvent was then evaporated to get a dry lipid film, which was then hydrated with liposome buffer (50 mM HEPES, 150 mM NaCl buffer at pH 7.4) to a final concentration 15 mg/ml lipid solution. The liposomes were formed by sonication in an ultrasound bath followed by flash-freeze in liquid nitrogen and slowly thaw in room temperature for 10 times cycles. The hydrated liposomes were further extruded by a lipid extruder (Avanti Polar Lipids Inc.) with 200 nm polycarbonate membranes (Avanti Polar Lipids) for 21 times.

Liposome-remodeling assay

Liposome-remodeling assay was performed as previous described with minor modifications [15]. Liposomes and the purified FAM134B-GST protein were mixed at an indicated lipid-to-protein ratio (LPR) and incubated for 18 h at 22 °C in 30 μL of liposome buffer with constant agitation (600 rpm). To investigate the effect of different LPS, FAM134B-GST protein was first added to liposome at LPR 100:1 for 1 h, then added LPS to

the proteoliposome and incubated for 17 h at 22 °C. All the samples were assessed by negative-stain transmission electron microscopy. For imaging, samples were first diluted to a final lipid concentration of 1 mg/ml by liposome buffer. 5 μl of each diluted sample was deposited to the carbon-coated copper grids (SPI Supplies), which were already glow-discharged for 20 s at 15 mA and 0.38 mbar vacuum. After 1 minute incubation and washes with buffer for twice, 1% uranyl formate was subsequently used to stain the grids for 10 seconds at room temperature. A 120 kV Tecnai Spirit Biotwin electron microscope (FEI) equipped with a 4k × 4k CCD detector (US4000-1, Gatan) was used to taken 10 micrographs for each sample. Image J software was used to measure the sizes (diameters) of 300 proteoliposomes for each sample.

OMV isolation

0.5 L overnight grown bacterial cultures were harvested for OMV isolation. Bacterial cells were first removed by centrifugation (12,000 g for 15 min), the supernatant was filtered through 0.45 μm PVDF membrane, the filtered broth concentrated to 50 ml (Vivaflow 200, 100,000 MWCO PES, Sartorius), and the OMVs were pelleted by ultracentrifugation at 60,000 rpm (369548.3 g) for 1 hr at 4 °C. The OMVs were washed with PBS and pelleted again by ultracentrifugation. The OMVs were resuspended in 0.5 ml PBS. In the cases which needed to do immunofluorescence labeling, Vybrant DiO cell labeling dye (ThermoFisher

Scientific) was added at 1:50 and incubated at 37 °C for 20 min. After labeling, the excess dye was removed and washed by PBS three times at 3000 rpm (956 g) by Micron 10 kDa centrifugal filter units (Millipore) in a benchtop centrifuge. The OMVs were further sterilized by syringe filters (0.22 um) and measured concentration by bicinchoninic acid assay (BCA) method. OMVs were added to the cells at concentration of 25 µg/ml.

Quantification and statistical analysis

GraphPad Prism 8 was used to do statistical analysis. Comparisons of two variables were analyzed by unpaired and two-tailed Student's t tests. For three or more sets of data, statistics were performed by one-way ANOVA with Tukey's multiple comparison post test. * indicates $p < 0.05$, ** indicates $p < 0.01$, *** indicates $p < 0.001$. N represents the number of independent biological replicates. Data are represented as mean ± sem.

Acknowledgements

We thank Prof. Dr. Volkhard A. J. Kempf at the Institute for Medical Microbiology and Infection Control, Hospital of the Goethe University for the kind gift of the EPEC O127:H6 strain. We thank the staff at the Quantitative Proteomics Unit at Goethe University for support with mass spectrometry and the Frankfurt Center for Advanced Microscopy (FCAM) for access to microscopes.

Funding

This research is supported by the Deutsche Forschungsgemeinschaft (DFG, German Research Foundation), project number 259130777-SFB 1177, the European Union (ERC, ER-REMODEL, 101055213), the HMWK-funded cluster grant ENABLE, and grants from Else Kroener Fresenius Stiftung and Dr. Rolf M. Schwiete Stiftung to ID. M.H. was supported by the DFG by project P8 in SFB1557 and HE1964/23-1 in priority program SPP 2225 'Exit Strategies'. C.A.H. was supported by the DFG HU 800/14-1. Y.L.C. was supported by funding through a National Science and Technology Council, project NSTC 113-2320-B-006-026 -, NSTC 112-2320-B-006-012-MY2 and MOST 108-2917-I-564-021.

Disclosure statement

The authors declare no competing interests.

Declaration of generative AI and AI-assisted technologies in the writing process

During the preparation of this work the author(s) used chatGPT in order to improve language and readability for some sentences. After using this tool, the authors reviewed and edited the content as needed and takes full responsibility for the content of the publication.

Data availability

The MS proteomics data have been deposited to the ProteomeXchange Consortium through the PRIDE partner repository with the dataset identifiers PXD053709.

References

[1] Escoll P, Mondino S, Rolando M, et al. Targeting of host organelles by pathogenic bacteria: a sophisticated subversion strategy. Nat Rev Microbiol. 2016;14(1):5-19.

[2] Gubas A, Dikic I. ER remodeling via ER-phagy. Mol Cell. 2022;82(8):1492-1500.
[3] Chino H, Mizushima N. ER-phagy: quality control and turnover of endoplasmic reticulum. Trends Cell Biol. 2020;30(5):384-398.
[4] Chino H, Mizushima N. ER-phagy: quality and quantity control of the endoplasmic reticulum by autophagy. Cold Spring Harb Perspect Biol. 2023;15(1).
[5] Khaminets A, Heinrich T, Mari M, et al. Regulation of endoplasmic reticulum turnover by selective autophagy. Nature. 2015;522(7556):354-8.
[6] Kumar D, Lak B, Suntio T, et al. RTN4B interacting protein FAM134C promotes ER membrane curvature and has a functional role in autophagy. Mol Biol Cell. 2021;32(12):1158-1170.
[7] Reggio A, Buonomo V, Berkane R, et al. Role of FAM134 paralogues in endoplasmic reticulum remodeling, ER-phagy, and collagen quality control. EMBO Rep. 2021;22(9):e52289.
[8] Grumati P, Morozzi G, Holper S, et al. Full length RTN3 regulates turnover of tubular endoplasmic reticulum via selective autophagy. Elife. 2017;6.
[9] Fumagalli F, Noack J, Bergmann TJ, et al. Translocon component Sec62 acts in endoplasmic reticulum turnover during stress recovery. Nat Cell Biol. 2016;18(11):1173-1184.
[10] Smith MD, Harley ME, Kemp AJ, et al. CCPG1 Is a non-canonical autophagy cargo receptor essential for ER-phagy and pancreatic ER proteostasis. Dev Cell. 2018;44(2):217-232 e11.
[11] Chen Q, Xiao Y, Chai P, et al. ATL3 Is a tubular ER-phagy receptor for GABARAP-mediated selective autophagy. Curr Biol. 2019;29(5):846-855 e6.
[12] An H, Ordureau A, Paulo JA, et al. TEX264 Is an endoplasmic reticulum-resident ATG8-interacting protein critical for ER remodeling during nutrient stress. Mol Cell. 2019;74(5):891-908 e10.
[13] Chino H, Hatta T, Natsume T, et al. Intrinsically disordered protein TEX264 mediates ER-phagy. Mol Cell. 2019;74(5):909-921 e6.
[14] Nthiga TM, Kumar Shrestha B, Sjottem E, et al. CALCOCO1 acts with VAMP-associated proteins to mediate ER-phagy. EMBO J. 2020;39(15):e103649.
[15] Bhaskara RM, Grumati P, Garcia-Pardo J, et al. Curvature induction and membrane remodeling by FAM134B reticulon homology domain assist selective ER-phagy. Nat Commun. 2019;10(1):2370.
[16] Siggel M, Bhaskara RM, Moesser MK, et al. FAM134B-RHD protein clustering drives spontaneous budding of asymmetric membranes. J Phys Chem Lett. 2021;12(7):1926-1931.
[17] Jiang X, Wang X, Ding X, et al. FAM134B oligomerization drives endoplasmic reticulum membrane scission for ER-phagy. EMBO J. 2020;39(5):e102608.

[18] Gonzalez A, Covarrubias-Pinto A, Bhaskara RM, et al. Ubiquitination regulates ER-phagy and remodelling of endoplasmic reticulum. Nature. 2023.

[19] Park BS, Song DH, Kim HM, et al. The structural basis of lipopolysaccharide recognition by the TLR4-MD-2 complex. Nature. 2009;458(7242):1191-5.

[20] Garcia-del Portillo F, Stein MA, Finlay BB. Release of lipopolysaccharide from intracellular compartments containing *Salmonella* typhimurium to vesicles of the host epithelial cell. Infect Immun. 1997;65(1):24-34.

[21] Shi J, Zhao Y, Wang Y, et al. Inflammatory caspases are innate immune receptors for intracellular LPS. Nature. 2014;514(7521):187-92.

[22] Aglietti RA, Estevez A, Gupta A, et al. GsdmD p30 elicited by caspase-11 during pyroptosis forms pores in membranes. Proc Natl Acad Sci U S A. 2016;113(28):7858-63.

[23] Ding J, Wang K, Liu W, et al. Pore-forming activity and structural autoinhibition of the gasdermin family. Nature. 2016;535(7610):111-6.

[24] Santos JC, Boucher D, Schneider LK, et al. Human GBP1 binds LPS to initiate assembly of a caspase-4 activating platform on cytosolic bacteria. Nat Commun. 2020;11(1):3276.

[25] Vanaja SK, Russo AJ, Behl B, et al. Bacterial outer membrane vesicles mediate cytosolic localization of LPS and caspase-11 activation. Cell. 2016;165(5):1106-1119.

[26] Silhavy TJ, Kahne D, Walker S. The bacterial cell envelope. Cold Spring Harb Perspect Biol. 2010;2(5):a000414.

[27] Schwechheimer C, Kuehn MJ. Outer-membrane vesicles from Gram-negative bacteria: biogenesis and functions. Nat Rev Microbiol. 2015;13(10):605-19.

[28] Juodeikis R, Carding SR. Outer membrane vesicles: biogenesis, functions, and issues. Microbiol Mol Biol Rev. 2022;86(4):e0003222.

[29] Adams PG, Lamoureux L, Swingle KL, et al. Lipopolysaccharide-induced dynamic lipid membrane reorganization: tubules, perforations, and stacks. Biophys J. 2014;106(11):2395-407.

[30] Wittig I, Braun HP, Schagger H. Blue native PAGE. Nat Protoc. 2006;1(1):418-28.

[31] Zenk SF, Jantsch J, Hensel M. Role of *Salmonella enterica* lipopolysaccharide in activation of dendritic cell functions and bacterial containment. J Immunol. 2009;183(4):2697-707.

[32] Madan R, Rastogi R, Parashuraman S, et al. *Salmonella* acquires lysosome-associated membrane protein 1 (LAMP1) on phagosomes from Golgi via SipC protein-mediated recruitment of host Syntaxin6. J Biol Chem. 2012;287(8):5574-87.

[33] LaRock DL, Chaudhary A, Miller SI. *Salmonellae* interactions with host processes. Nat Rev Microbiol. 2015;13(4):191-205.

[34] Wild P, Farhan H, McEwan DG, et al. Phosphorylation of the autophagy receptor

optineurin restricts *Salmonella* growth. Science. 2011;333(6039):228-33.
[35] Ravenhill BJ, Boyle KB, von Muhlinen N, et al. The cargo receptor NDP52 initiates selective autophagy by recruiting the ULK complex to cytosol-invading bacteria. Mol Cell. 2019;74(2):320-329 e6.
[36] Perrin AJ, Jiang X, Birmingham CL, et al. Recognition of bacteria in the cytosol of mammalian cells by the ubiquitin system. Curr Biol. 2004;14(9):806-11.
[37] Deatherage BL, Lara JC, Bergsbaken T, et al. Biogenesis of bacterial membrane vesicles. Mol Microbiol. 2009;72(6):1395-407.
[38] Nevermann J, Silva A, Otero C, et al. Identification of genes involved in biogenesis of outer membrane vesicles (OMVs) in *Salmonella enterica* Serovar Typhi. Front Microbiol. 2019;10:104.
[39] Szczepaniak J, Press C, Kleanthous C. The multifarious roles of Tol-Pal in Gram-negative bacteria. FEMS Microbiol Rev. 2020;44(4):490-506.
[40] Kawasaki K, Ernst RK, Miller SI. 3-O-deacylation of lipid A by PagL, a PhoP/PhoQ-regulated deacylase of *Salmonella* typhimurium, modulates signaling through Toll-like receptor 4. J Biol Chem. 2004;279(19):20044-8.
[41] Elhenawy W, Bording-Jorgensen M, Valguarnera E, et al. LPS remodeling triggers formation of outer membrane vesicles in *Salmonella*. mBio. 2016;7(4).
[42] Gatica D, Alsaadi RM, El Hamra R, et al. The ER-phagy receptor FAM134B is targeted by *Salmonella* Typhimurium to promote infection. Nat Commun. 2025;16(1):2923.
[43] Moretti J, Roy S, Bozec D, et al. STING senses microbial viability to orchestrate stress-mediated autophagy of the endoplasmic reticulum. Cell. 2017;171(4):809-823 e13.
[44] Kutsch M, Sistemich L, Lesser CF, et al. Direct binding of polymeric GBP1 to LPS disrupts bacterial cell envelope functions. EMBO J. 2020;39(13):e104926.
[45] Santos NC, Silva AC, Castanho MA, et al. Evaluation of lipopolysaccharide aggregation by light scattering spectroscopy. Chembiochem. 2003;4(1):96-100.
[46] Meunier E, Dick MS, Dreier RF, et al. Caspase-11 activation requires lysis of pathogen-containing vacuoles by IFN-induced GTPases. Nature. 2014;509(7500):366-70.
[47] Man SM, Karki R, Sasai M, et al. IRGB10 liberates bacterial ligands for sensing by the AIM2 and caspase-11-NLRP3 inflammasomes. Cell. 2016;167(2):382-396 e17.
[48] Datsenko KA, Wanner BL. One-step inactivation of chromosomal genes in Escherichia coli K-12 using PCR products. Proc Natl Acad Sci U S A. 2000;97(12):6640-5.
[49] Hoffmann S, Schmidt C, Walter S, et al. Scarless deletion of up to seven methyl-accepting chemotaxis genes with an optimized method highlights key function of

CheM in *Salmonella* Typhimurium. PLoS One. 2017;12(2):e0172630.
[50] Steele-Mortimer O. Infection of epithelial cells with *Salmonella* enterica. Methods Mol Biol. 2008;431:201-11.

Figure legends

Figure 1. *Salmonella* LPS activates FAM134B-mediated ER fragmentation. (A) Immunofluorescence staining of HA, *Salmonella* LPS, and LC3B in HeLa TREx inducible cell lines expressing FLAG-HA-FAM134B that were infected with SL1344 for 2 hr. DAPI staining was used for cell nuclear and bacteria DNA staining. Arrows indicate the puncta with colocalization of HA-FAM134B and *Salmonella* LPS or LC3B, and arrowheads indicate the puncta with colocalization of HA-FAM134B, *Salmonella* LPS and LC3B. Scale bar, 10 μm. The histogram showed the florescence intensity and the location of HA-FAM134B (green), LC3B (red), and *Salmonella* LPS (magenta) of the white line in the image, which analyzed by image J. (B) Quantification of HA and *Salmonella* LPS staining in HeLa TREx inducible cell lines expressing FLAG-HA-FAM134B infected with SL1344 for 2 hr and 8 hr. The percentage of FAM134B-positive (+) and FAM134B-negative (-) LPS puncta in all LPS puncta were quantified using CellPathfinder software. Data presented as mean + standard error of the mean (sem), n=3, > 400 cells. (C) Number of LC3B-positive HA-FAM134B puncta in HeLa TREx inducible cell lines expressing wild type (WT) or LIR mutant (mtLIR) FLAG-HA-FAM134B infected with SL1344 for 2 hr. Representative images are shown in Figure S1D. (D) Co-IP of endogenous LC3B-II with HA in HeLa TREx inducible cells

without doxycycline (Dox) treatment or with FLAG-HA-FAM134B WT or FLAG-HA-FAM134B mtLIR after Dox treatment. The cells were infected with SL1344 for 2 hr and pretreated with 200 ng/ml Bafilomycin A1 (BafA1) for 3 hr. GAPDH was used as an internal control of input. (E and F) Immunofluorescence staining and quantification of HA, *Salmonella* LPS, and LC3B in HeLa TREx inducible cell lines expressing FLAG-HA-FAM134B transfected with 1 μg/ml *Salmonella* LPS for 18 hr by lipofectamine 2000. Lipo, lipofectamine only. (E) Arrowheads indicate the puncta with colocalization of HA-FAM134B, *Salmonella* LPS and LC3B. The histogram showed the florescence intensity and the location of HA-FAM134B (green), LC3B (red), and *Salmonella* LPS (magenta) of the white line in the image, which analyzed by image J. Scale bar, 10 μm. (F) Quantification of LC3B-positive HA-FAM134B puncta per cell. (C and F) Solid bars of boxes indicate the medians. Boxes represent interquartile range from 25th to 75th percentile, and whiskers indicates 10th to 90th percentile. Differences were statistically analyzed by one-way ANOVA and Tukey's multiple comparison test. Data were collected 60 cells from three independent biological replicates. $^{**}p < 0.01$, $^{***}p < 0.001$. ns, not significant.

Figure 2. LPS binds to FAM134B via lipid A moiety. (A) Schematic representation of streptavidin pulldown assays. (B) Streptavidin pulldown assays that determine the binding of the indicated amounts of biotin-conjugated *E. coli* O111:B4 LPS and HA-tagged FAM134B

or RTN3L in FLAG-HA-FAM134B- or FLAG-HA-RTN3L-expressing HeLa TREx cell lysates. GAPDH was used as an internal control of input. (C) Streptavidin pulldown assays that determine the binding of the biotin-conjugated *E. coli* O111:B4 LPS to the endogenous protein of the ER-phagy receptors, FAM134B, RTN3L and TEX264 in HeLa cell lysates. GAPDH was used as an internal control of input. (D) Co-IP of LPS with HA in HeLa TREx inducible cell lines without Dox treatment or expressing FLAG-HA-FAM134B or FLAG-HA-RTN3L by Dox treatment, which were infected with SL1344 for 2 hr. GAPDH was used as an internal control of input. (E) Schematic representation of the LPS structure and the segments of different mutant variants of LPS, including lipid A, Re-LPS, Ra-LPS, and smooth (S)-LPS. P, phosphate; KDO, 3-deoxy-D-*manno*-octulosonic acid; Hep, L-*glycero*-D-*manno*-heptose; PEtn, phosphatidyl-ethanolamine; Glc, D-glucose; Gal, D-galactose; GlcNac, N-acetyl-D-glucosamine. (F) Unlabeled S-LPS, Ra-LPS, Re-LPS, lipid A, and muramyl dipeptide (MDP) were used for competition with the binding of biotin-conjugated *E. coli* O111:B4 LPS to HA-tagged FAM134B in Dox-induced FLAG-HA-FAM134B HeLa TREx cell lysates. (G) Indicated concentrations of polymyxin B (Poly B) were used to inhibit the binding of biotin-conjugated *E. coli* O111:B4 LPS to HA-tagged FAM134B in Dox-induced FLAG-HA-FAM134B HeLa TREx cell lysates.

Figure 3. FAM134B binds to LPS via electrostatic forces. (A) Schematic representation of the full length FAM134B sequence, which is composed of a reticulum homology domain

(RHD), N-terminal (Nter, grey) and C-terminal regions (Cter, grey). LC3-interacting region consisting of 4 amino acids (LIR, pink) is located in the C-terminal region. The RHD consists of two transmembrane segments TM12 and TM34 (green), which are connected by a 60-residue linker, and two additional terminal segments. The C-terminal fragment of the RHD (AHC, yellow) and the linker-helix (AHL, yellow) form conserved amphipathic helices. The lower table shows the number of positively charged residues (arginine, R; Lysine, K) and the percentage of solvent accessible in every segment of FAM134B. (B) Substitution of amino acids (R or K to glutamic acid, E) in segment AHL (AHLmt), AHC (AHCmt), and C-terminal (CTERmt). DOUBLEmt 1, DOUBLEmt 2, and TRIPLEmt indicate combination as shown in the table. (C) Streptavidin pulldown assays that determine the binding of the indicated amount of biotin-conjugated *E. coli* O111:B4 LPS to HA-tagged wild type or different mutant FAM134B transfected in HEK293T cells. GAPDH was used as an internal control of input. (D and E) Immunofluorescence staining and quantification of HA and *Salmonella* LPS, and LC3B in FAM134B WT-HA or FAM134B TRIPLEmt-HA transfected HeLa cells infected with SL1344 for 2 hr. Scale bar, 10 μm. (E) Quantification of number of LC3B-positive HA-FAM134B puncta per cell. Solid bars of boxes indicate the medians. Boxes represent interquartile range from 25th to 75th percentile, and whiskers indicates 10th to 90th percentile. Differences were statistically analyzed by one-way ANOVA and Tukey's multiple comparison test. ***$p < 0.001$. ns, not significant. Data were collected 60 cells from three independent

biological replicates. (F) Co-IP of LPS and endogenous LC3B-II in FAM134B WT-HA or FAM134B TRIPLEmt-HA transfected HeLa cells, which were infected with SL1344 for 2 hr. GAPDH was used as an internal control of input. The bands at ~ 22kD is the light chain of the antibody used for Co-IP.

Figure 4. O-Ag of LPS induces FAM134B oligomerization and membrane fragmentation. (A) Size analysis of S protein-FLAG-Streptavidin binding peptide (SFB)-FAM134B oligomers after incubation with indicated amount of *Salmonella* S-LPS or lipid A by blue native page and immunoblotting of FLAG. (B) Size analysis of SFB-FAM134B oligomers purified from cell lysates infected with NCTC12023 WT or O-Ag mutant (Δ) and complemented (compl.) strains. Upper panel shows lower exposure (Low exp) blot and lower blot shows higher exposure (high exp) blot. GAPDH was used as an internal control of input. (C) Schematic representation of LPS structure of different O-Ag mutant strains, including the strains mutant for *rfbP*, *rfaL*, *rfaG*, and *rfaH*. (D and E) Representative images (D) and quantitative results (E) of remodeled proteoliposomes (scale bars, 100 nm) taken from negative stain Transmission Electron Microscopy (nsTEM). Empty liposomes (Empty) were added FAM134B-GST recombinant protein at a lipid to protein ratio (LPR) 100:1 without (LPR 100:1) or with 0.5 mg/ml LPS (LPR 100:1+LPS 0.5) or 1 mg/ml LPS (LPR 100:1+ LPS 1). Incubation of liposome with 1 mg/ml LPS was taken as negative control to check the

effect of LPS on liposome. The diameter of the representative proteoliposome with average size for each group showed by dotted line or arrow. (F and G) Representative images (F) and quantitative results (G) of different LPS, including 1 mg/ml of S-LPS, Ra-LPS, and Re-LPS, remodeled proteoliposomes (LPR 100:1, scale bars, 100 nm). The diameter of the representative proteoliposome with average size for each group showed by dotted line or arrow. (E and G) The size distributions (n=300 each) from nsTEM images were measured and showed by violin plots, showing a central boxplot (black lines indicate median with interquartile range) with mirrored histograms on both sides (G). (H and I) Immunofluorescence of HA, *Salmonella* LPS, and LC3B in HeLa TREx inducible cell line expressing FLAG-HA-FAM134B infected with NCTC12023 WT or LPS O-Ag mutant (Δ) and complemented (compl.) strains for 2 hr (H). DAPI staining was used for cell nuclear and bacterial DNA staining. Scale bar, 10 μm. Quantification of LC3B-positive HA-FAM134B puncta per cell (H) and *Salmonella* count per cell (I). Data were collected 60 cells from three independent biological replicates. Representative images are shown in Extended Data Fig. 3c. (E,G,H,I) Differences were statistically analyzed by one-way ANOVA and Tukey's multiple comparison test. *$p<0.05$, **$p<0.01$, ***$p < 0.001$, ns not significant.

Figure 5. FAM134B promotes xenophagosomes formation and GAS clearance. (A) Immunofluorescence staining of HA, LC3B, and LAMP1 in HeLa TREx inducible cell line

expressing FLAG-HA-FAM134B infected with SL1344 for 4 hr. DAPI was used for cell nuclear and bacterial DNA staining. Scale bar, 10 μm. (B and C) The percentage of FAM134B-, LC3B-, or LAMP-1-positive Salmonella in total Salmonella (B), as well as the percentage of FAM134B and LC3B double-positive Salmonella in all LC3B-positive Salmonella and the percentage of FAM134B and LAMP1 double-positive Salmonella in all LAMP1-positive Salmonella (C) was quantified using CellPathfinder software. Data presented as mean + sem, n=3, > 400 cells. Differences were statistically analyzed by one-way ANOVA and Tukey's multiple comparison test. ***$p < 0.001$, ns, not significant. (D and E) Immunofluorescence staining of LC3B and REEP5 in FAM134B WT HeLa and FAM134B KO HeLa infected with SL1344 for 4 hr (D). DAPI was used for cell nuclear and bacterial DNA staining. Scale bar, 10 μm. Quantification of LC3-positive Salmonella per cell (E). Data were collected 60 cells. Differences were statistically analyzed by unpaired t-test. ***$p < 0.001$. (F) Colony-forming assay was performed to quantify the bacteria count in FAM134B WT HeLa and FAM134B KO HeLa infected with SL1344 100 moi at the indicated time points. Data collected from three independent biological replicates. (G) Representative image of HeLa cells infected with pHut-gfp Salmonella bacteria after infection (GFP-expressing bacteria are cytosolic, right; vacuolar bacteria have no GFP signal, left). Scale bar 10μm. (H) Quantification of GFP-expressing pHut-gfp Salmonella bacteria (cytosolic) after infection with moi 100 of FAM134B WT HeLa and FAM134B KO HeLa at the indicated time points.

Data collected for >100 cells from three independent biological replicates. (F, H) Differences were statistically analyzed by two-way ANOVA and Šidák correction for multiple comparisons. **p<0.01, ns not significant.

Figure 6. LPS for FAM134B-mediated fragmentation is delivered by OMV. (A and B) Immunofluorescence staining of HA, *Salmonella* LPS, and LC3B in cells infected with different mutant strains, including Δ*ompA*, Δ*tolAB*, and Δ*degS*, and Δ*pagL* strains. DAPI was used for cell nuclear and bacterial DNA staining. Scale bar, 10 μm. Quantification of LC3B-positive HA-FAM134B puncta (A) and *Salmonella* count per cell (B). Representative images are shown in Figure S5D. (C) Co-IP of LPS with HA in cells infected with NCTC12023 WT or indicated mutant strains for 2 hr. GAPDH was used as an internal control of input. (D and E) Immunofluorescence staining of HA, *Salmonella* LPS, and LC3B in cells treated with purified SL1344 OMVs for 6 hr (D). DAPI was used for cell nuclear DNA staining. Scale bar, 10 μm. Quantification of LC3B-positive HA-FAM134B puncta per cell (E). (F) Immunofluorescence staining of HA and LC3B in cells treated with purified OMVs form NCTC12023 WT or indicated mutant strains for 6 hr. DAPI was used for cell nuclear DNA staining. Scale bar, 10 μm. Quantification of LC3B-positive HA-FAM134B puncta per cell. (G and H) Immunofluorescence staining of HA and LC3B in cells infected by EPEC or BL21 directly or with 0.45 μm transwell for 4 hr (G). DAPI was used for cell nuclear DNA staining.

Scale bar, 10 μm. Quantification of LC3B-positive HA-FAM134B puncta per cell (H). (I) Immunofluorescence staining of HA and LC3B in cells treated with purified OMVs form EPEC or BL21 for 6 hr. Quantification of LC3B-positive HA-FAM134B puncta per cell with OMVs, stained by DiO Vybrant. Representative images are shown in Figure S6B. HeLa TREx inducible cell lines expressing FLAG-HA-FAM134B was used for all experiments in Figure 6. (A, B, E, F, H, and I) Solid bars of boxes indicate the medians. Boxes represent interquartile range from 25th to 75th percentile, and whiskers indicates 10th to 90th percentile. Differences were statistically analyzed by one-way ANOVA and Tukey's multiple comparison test. ***$p < 0.001$, ns, not significant. Data were collected 60 cells from two (A, B and H) three independent (E, F and I) biological replicates.

Figure 7. A hypothetical model. Cytosolic LPS binds to the ER-phagy receptor FAM134B, triggering oligomerization of FAM134B and ER fragmentation, and subsequently, the formation of FAM134B and ER membrane-positive xenophagosome for bacterial clearance. The figure was created by Inkscape.

Figure 1 Cheng et al

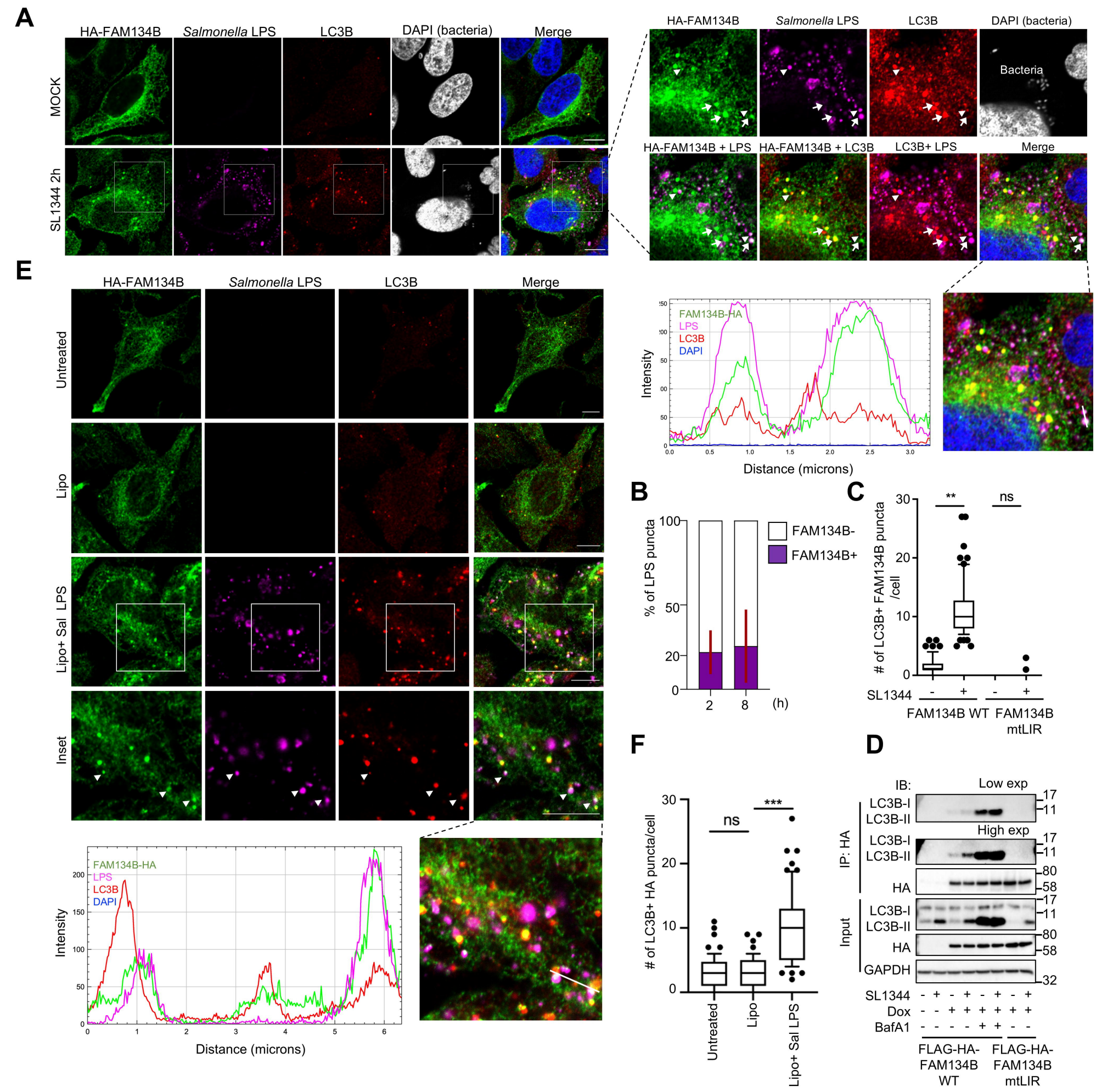

Figure 2 Cheng et al

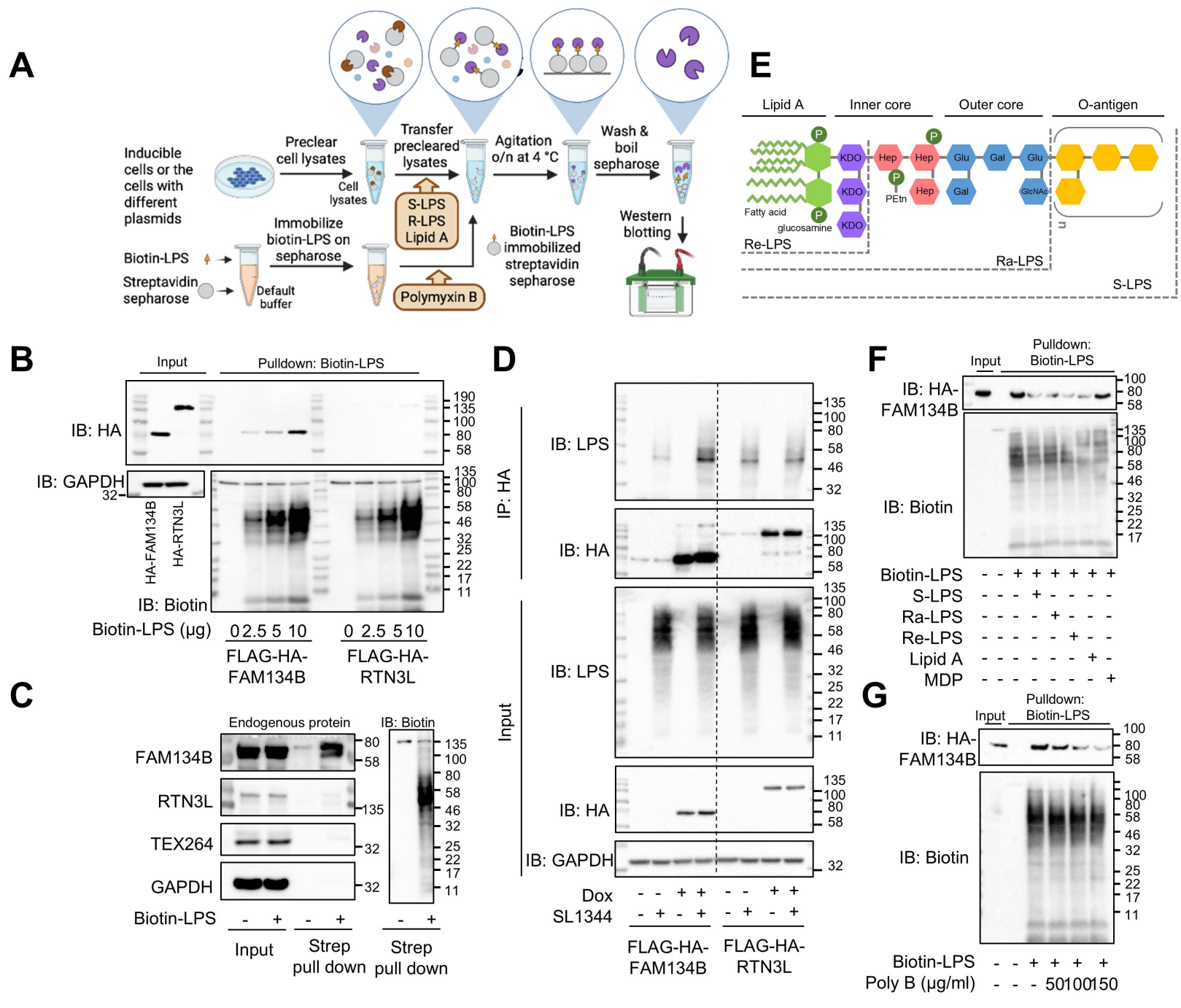

Figure 3 Cheng et al

A

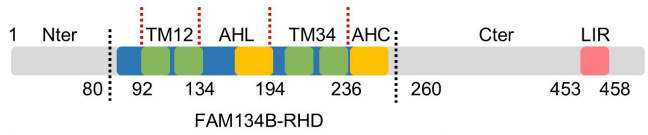

Domain (Residue #)	Positively Charged Residues (R+K)	% Solvent Accessible
Nter (1-92)	4	4
TM 12 (92-134)	4	0
AHL (134-194)	7	11
TM34 (195-236)	2	0
AHC (237-260)	4	17
Cter (261-497)	18	7.6

B

AHLmt: FAM134B-AHLmt-HA
(R140E, R142E, R148E, K160E, R164E, R166E, K189E, K195E)

AHCmt: FAM134B-AHCmt-HA
(K241E, K245E, K247E, K252E, K264E, K265E, R266E, R268E, K273E, K275E, K278E, K291E, K299E)

CTERmt: FAM134B-CTERmt-HA
(K374E, R375E, K376E, K377E)

DOUBLEmt 1: AHLmt + AHCmt

DOUBLEmt 2: AHLmt + CTERmt

TRIPLEmt: AHLmt + AHCmt + CTERmt

C

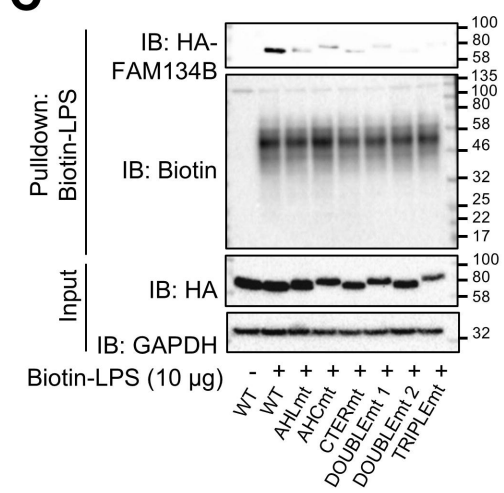

D

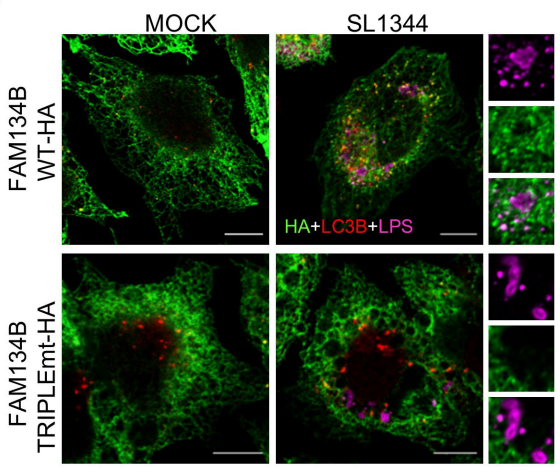

E

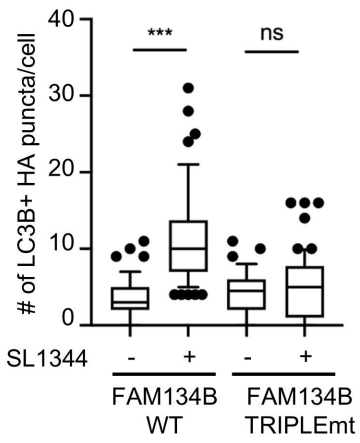

F

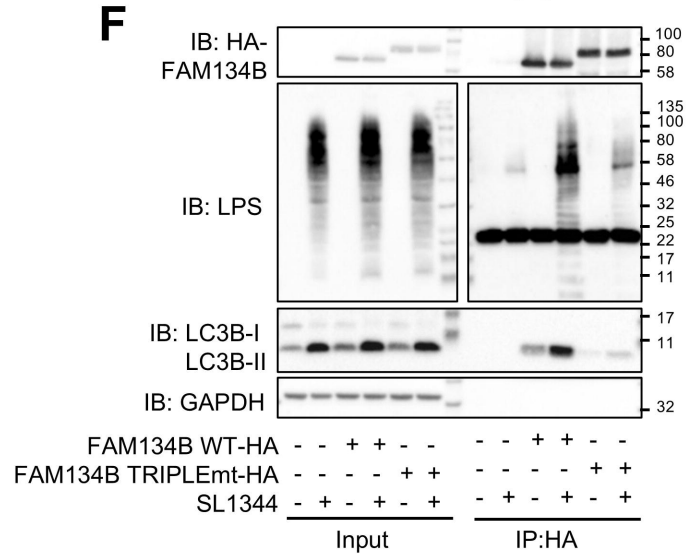

Figure 4 Cheng et al

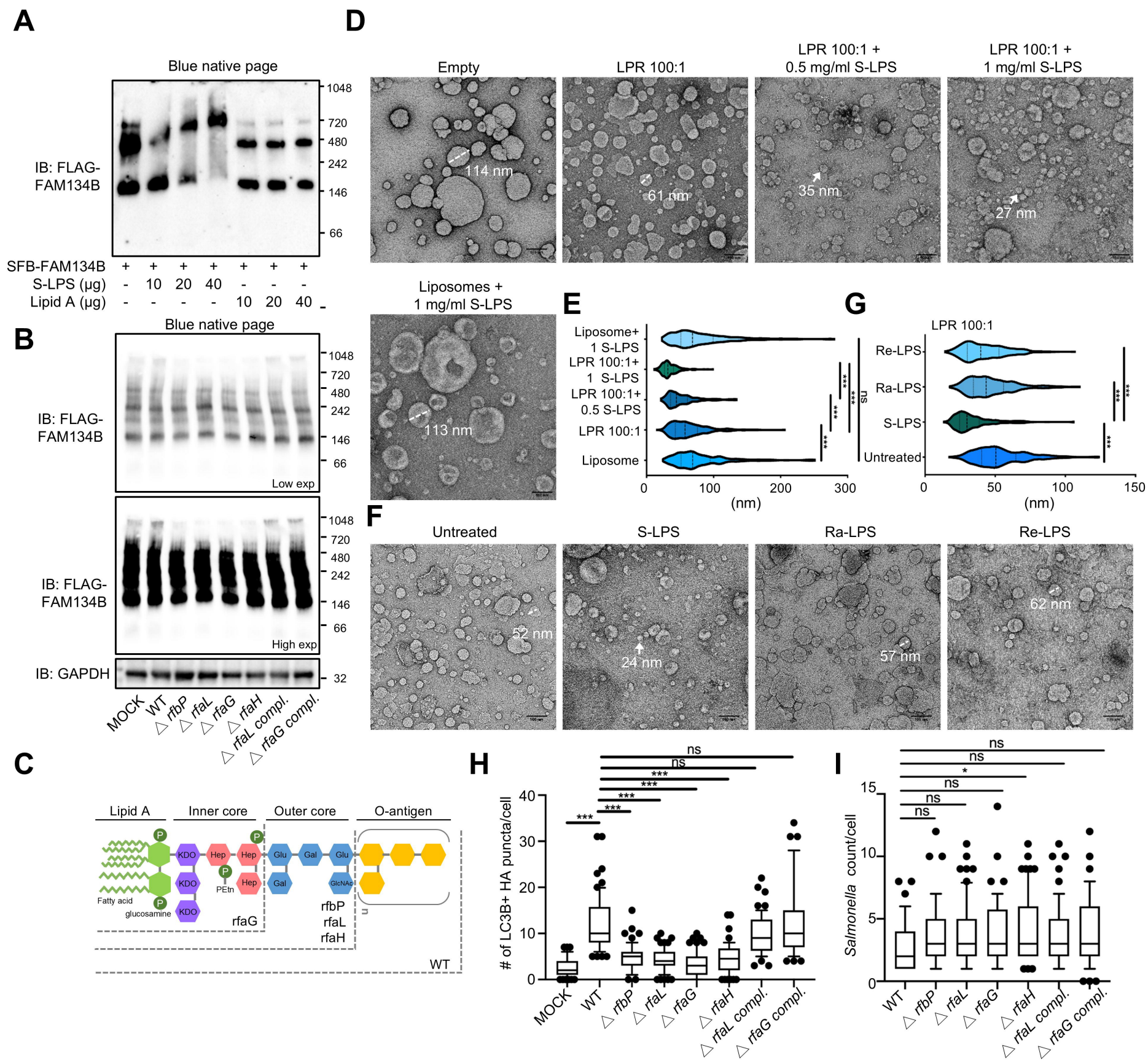

Figure 5 Cheng et al

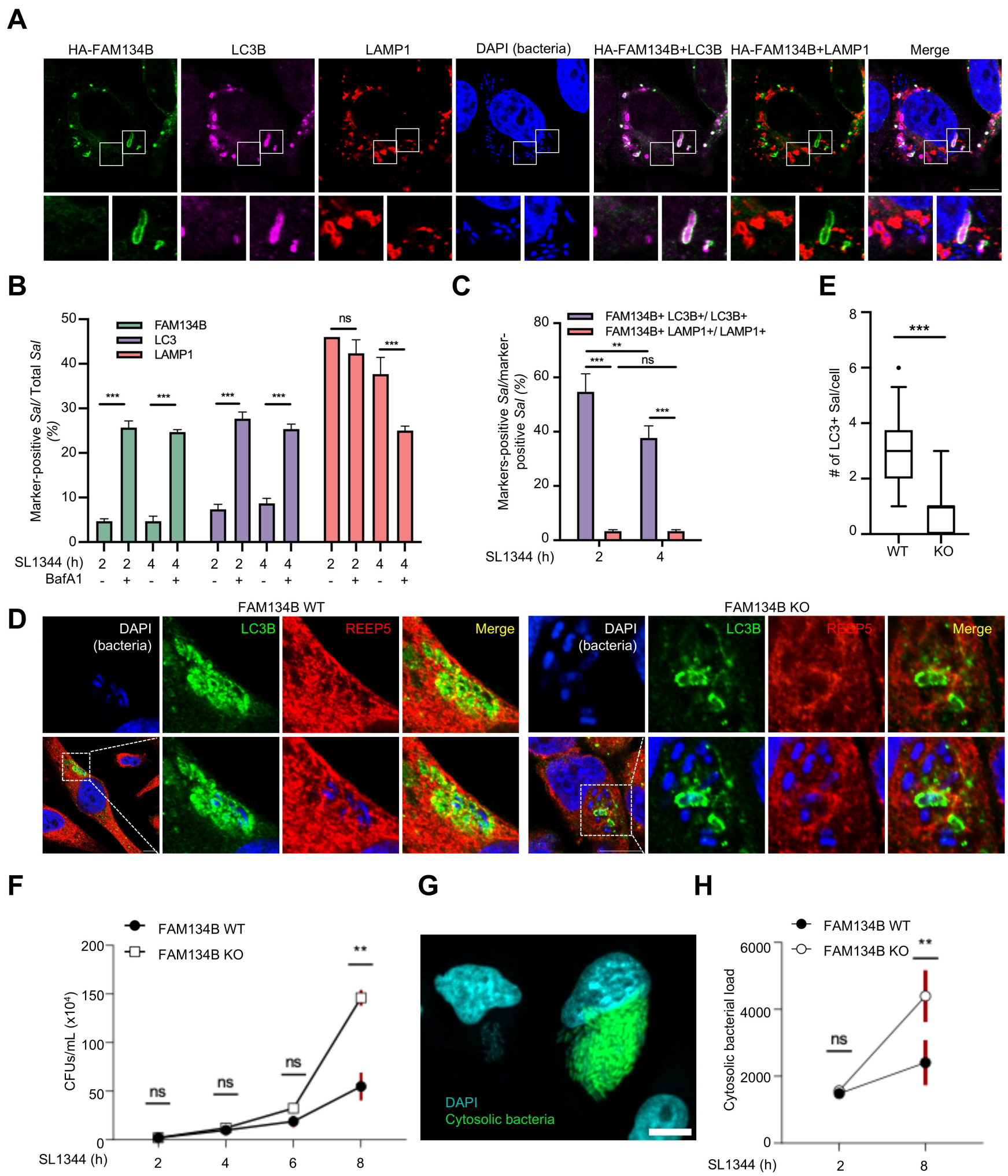

Figure 6 Cheng et al

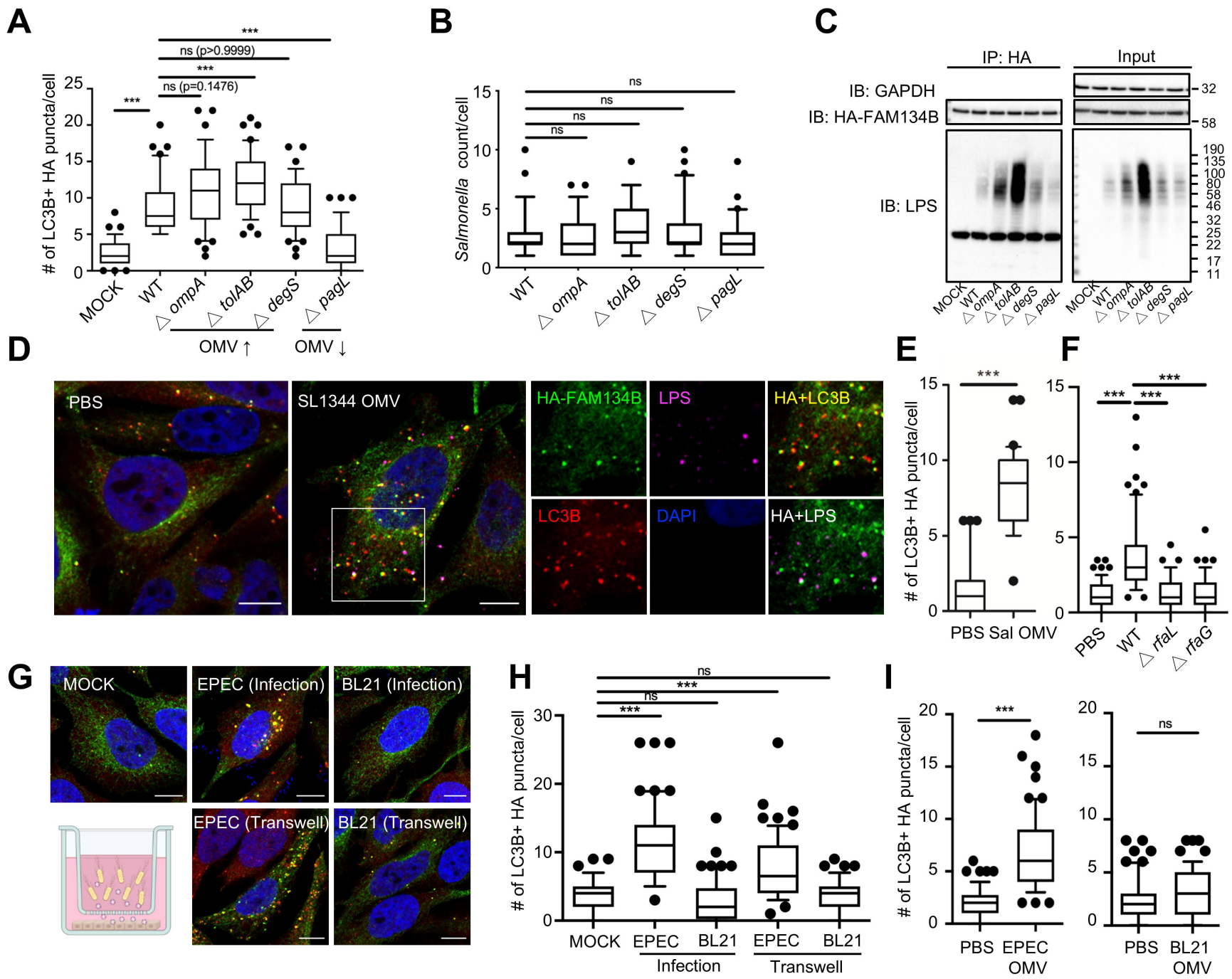
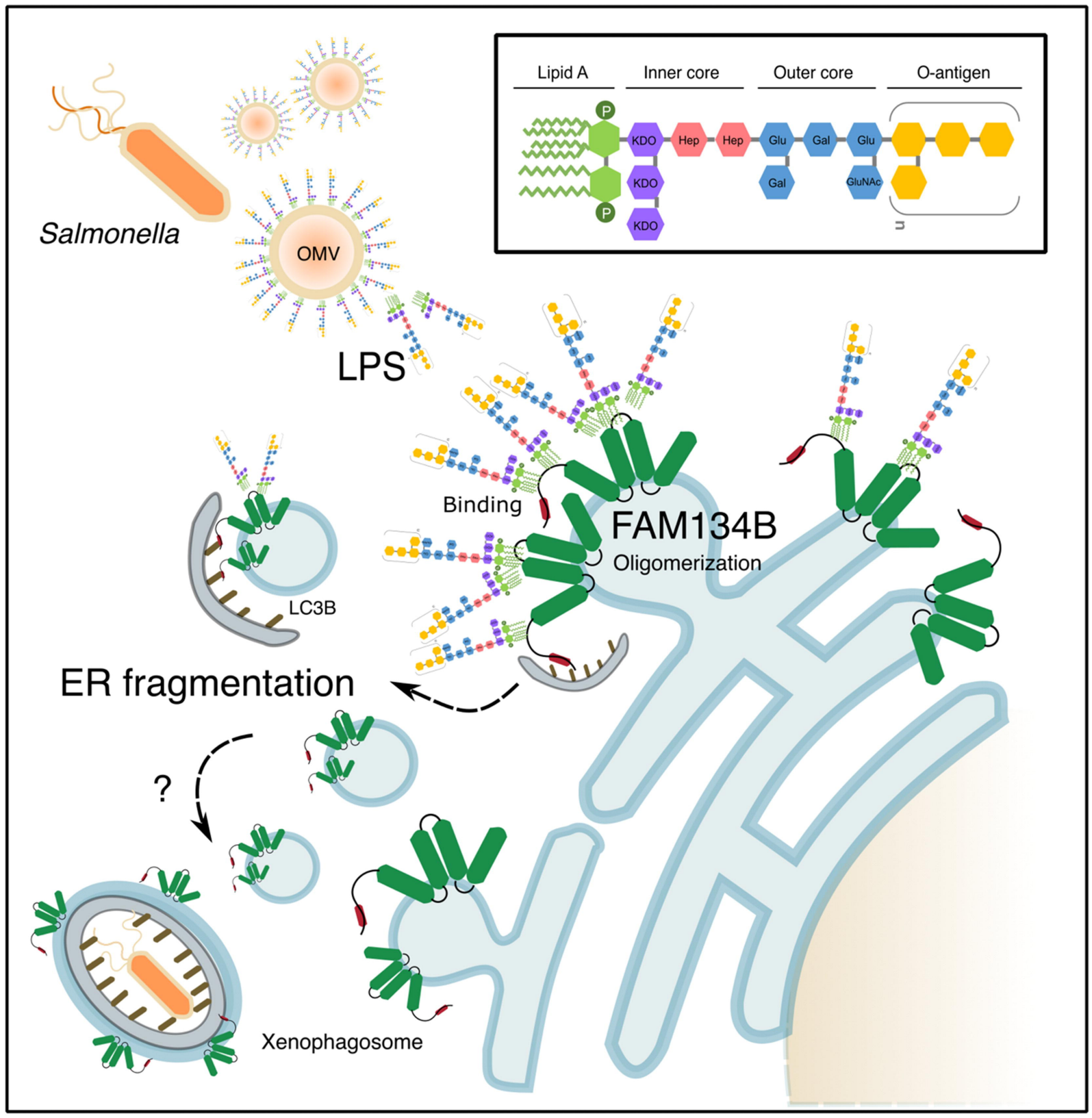
Figure 7 Cheng et al